JPET Fast Forward. Published on December 4, 2020 as DOI: 10.1124/jpet.120.000353
This article has not been copyedited and formatted. The final version may differ from this version.

Title Page

Title:

Increased levels of renal lysophosphatidic acid in rodent models with renal disease.

Authors:

Takashi Hirata, Stanley V. Smith, Teisuke Takahashi, Noriyuki Miyata, Richard J. Roman

Affiliate:

Department of Pharmacology and Toxicology, University of Mississippi Medical Center, Jackson, MS (T.H., S.V.S, R.J.R.)

Pharmacology Laboratories (T.H., T.T.), Research Headquarters of Pharmaceutical Operation (N.M.), Taisho Pharmaceutical Co., Ltd., Saitama, Japan

JPET Fast Forward. Published on December 4, 2020 as DOI: 10.1124/jpet.120.000353
This article has not been copyedited and formatted. The final version may differ from this version.

Running Title Page

Running Title:

LPA and renal disease

Corresponding Author:

Dr. Richard J. Roman, Department of Pharmacology and Toxicology, University of Mississippi Medical Center, 2500 North State Street, Jackson, MS 39216.

Telephone: (601) 984-1602

Fax: (601) 984-1637

E-mail: rroman@umc.edu

The number of text pages: 38

The number of tables: 3

The number of figures: 7

The number of References: 45

The number of words in the Abstract: 244

The number of words in the Introduction: 744

The number of words in the Discussion: 1498

Abbreviations:

CKD, chronic kidney disease; Dahl S, Dahl salt-sensitive; ESRD, end-stage renal disease; GFR, glomerular filtration rate; HbA1c, glycosylated hemoglobin; LC/MS/MS, liquid chromatography/mass spectrometry/mass spectrometry; LPA, lysophosphatidic acid; LPP, lipid phosphate phosphatase; PLA1, phospholipase A_1; PLA2, phospholipase A_2; SD, Sprague-Dawley; STZ, streptozotocin; T2DN, type 2 diabetic nephropathy; UUO,

JPET Fast Forward. Published on December 4, 2020 as DOI: 10.1124/jpet.120.000353
This article has not been copyedited and formatted. The final version may differ from this version.

unilateral ureteral obstruction

Recommended Section: Gastrointestinal, Hepatic, Pulmonary, and Renal

JPET Fast Forward. Published on December 4, 2020 as DOI: 10.1124/jpet.120.000353
This article has not been copyedited and formatted. The final version may differ from this version.

Abstract

Lysophosphatidic acid (LPA) is a bioactive lipid mediator that has been implicated in the pathophysiology of kidney disease. However, few studies have attempted to measure changes in the levels of various LPA species in the kidney following the development of renal disease. The present study measured the renal LPA levels during the development of kidney disease in rat models of hypertension, diabetes, and obstructive nephropathy, using liquid chromatography/mass spectrometry/mass spectrometry (LC/MS/MS). LPA levels (sum of 16:0, 18:0, 18:1, 18:2, and 20:4 LPA) were higher in the renal cortex of hypertensive Dahl salt-sensitive (Dahl S) rats fed a high salt diet than in normotensive rats fed a low salt diet (296.6 ± 22.9 versus 196.3 ± 8.5 nmol/g protein). LPA levels were elevated in the outer medulla of the kidney of streptozotocin-induced type 1 diabetic Dahl S rats compared with control rats (624.6 ± 129.5 versus 318.8 ± 17.1 nmol/g protein). LPA levels were also higher in the renal cortex of 18-month-old, type 2 diabetic nephropathy (T2DN) rats with more severe renal injury than in 6-month-old T2DN rats (184.9 ± 20.9 versus 116.9 ± 6.0 nmol/g protein). LPA levels also paralleled the progression of renal fibrosis in the renal cortex of SD rats following unilateral ureteral obstruction (UUO). Administration of a LPA receptor antagonist, Ki16425, reduced the degree of renal fibrosis in UUO rats. These results suggest that the production of renal LPA increases during the development of renal injury and contribute to renal fibrosis.

JPET Fast Forward. Published on December 4, 2020 as DOI: 10.1124/jpet.120.000353
This article has not been copyedited and formatted. The final version may differ from this version.

Significance Statement

The present study reveals that the LPA levels increase in the kidney in rat models of hypertension, diabetes, and obstructive nephropathy and administration of a LPA receptor antagonist attenuates renal fibrosis. Therapeutic approaches that target the formation or actions of renal LPA might be renoprotective and have therapeutic potential.

JPET Fast Forward. Published on December 4, 2020 as DOI: 10.1124/jpet.120.000353
This article has not been copyedited and formatted. The final version may differ from this version.

Introduction

Diabetes and hypertension are the leading causes of chronic kidney disease (CKD). The Global Burden of Disease database estimates that 276 million people had CKD in 2016 (Xie et al., 2018). CKD patients are at high risk for cardiovascular death and are more likely to develop the end-stage renal disease (ESRD) (Gansevoort et al., 2013; Tonelli et al., 2006). Although therapeutic interventions such as inhibition of the renin-angiotensin system, and tight control of blood glucose and blood pressure slow the progression of renal disease, the prevalence of ESRD continues to rise (Sharma and Sarnak, 2017). Therefore, there is an unmet need for novel and effective therapies to arrest the progression of CKD.

Lysophosphatidic acid (LPA) is a bioactive phospholipid that regulates multiple cell functions, including cell proliferation, migration, differentiation, and survival (Aikawa et al., 2015). LPA consists of a glycerol backbone with a phosphate group at the sn-3 position and a single fatty acyl chain at the sn-1 or sn-2 position. There are various species of LPA that differ in the length and degree of saturation of the fatty acyl chains. Previous studies have demonstrated that various LPA species have different biologic effects (Bandoh et al., 2000; Hayashi et al., 2001). To date, two major pathways of LPA production are known (Aoki et al., 2008; Nakanaga et al., 2010). Extracellular LPA is generated from lysophosphatidylcholine by the phospholipase D activity of autotaxin. Intracellular LPA is generated from phosphatidic acid by phospholipase A_1 (PLA1) or PLA2. On the other hand, the main pathway for LPA degradation involves its dephosphorylation by lipid phosphate phosphatases (LPP1 to LPP3) (Benesch et al., 2016). The local LPA concentration in tissue is tightly controlled by a balance of production and degradation of LPA through these enzymes. LPA acts through specific G protein-coupled receptors. So far, at least six LPA receptors have been identified (LPA_1 to LPA_6) (Mutoh et al., 2012).

LPA exerts various biological effects on different renal cell types, including

JPET Fast Forward. Published on December 4, 2020 as DOI: 10.1124/jpet.120.000353
This article has not been copyedited and formatted. The final version may differ from this version.

proximal tubular cells, mesangial cells, and fibroblasts (Inoue et al., 1997; Inoue et al., 1995; Fang et al., 2000; Geng et al., 2012). Several investigators have suggested that LPA stimulates mesangial cell proliferation and contraction, and contribute to the pathogenesis of glomerular disease (Inoue et al., 1997; Inoue et al., 1999). Others have reported that the expression of LPA_1 is increased in the kidney of unilateral ureteral obstruction (UUO) mice and genetic deletion or pharmacological inhibition of the LPA_1 decreased renal interstitial fibrosis (Pradère et al., 2007; Swaney et al., 2011). More recently, the dual $LPA_{1/3}$ antagonist, BMS002, was reported to reduce some of the features of diabetic nephropathy including albuminuria, glomerulosclerosis, renal fibrosis, and the fall in glomerular filtration rate (GFR) in type 2 diabetic db/db mice (Zhang et al., 2017). These observations suggest the involvement of LPA in the pathophysiology of various forms of renal disease.

LPA is present in various tissues and biological fluids, including the kidney, blood, and urine (Meleh et al., 2007; Grove et al., 2014). LPA is rapidly released from activated platelets and injured cells following inflammation, thrombosis, and tissue injury. They are proposed to contribute to the inflammatory and proliferative responses to injury (Dohi et al., 2012; Eichholtz et al., 1993). In this regard, it is reported that the concentration of LPA in the effluent from the pelvis of a ligated kidney is higher than in the urinary bladder of UUO-treated rats (Tsutsumi et al., 2011). More recently, Mirzoyan et al. reported that urinary LPA concentrations increased following 5/6 nephrectomy in mice when compared to sham control animals. The elevated concentration of LPA was significantly correlated with albuminuria and the degree of renal tubulointerstitial fibrosis (Mirzoyan et al., 2016). A recent clinical study has also found that urinary LPA concentrations are increased in diabetic patients and was associated with albuminuria (Saulnier-Blache et al., 2017). These findings indicate that renal LPA production is altered during the development of renal injury, and increases in renal LPA may contribute to the pathophysiology of renal disease.

JPET Fast Forward. Published on December 4, 2020 as DOI: 10.1124/jpet.120.000353
This article has not been copyedited and formatted. The final version may differ from this version.

However, little information is available regarding changes in the levels of various LPA species in the kidney in different models of renal disease. Therefore, this study examined the renal LPA levels during the development of renal injury in rat models of hypertension, diabetes, and obstructive nephropathy using liquid chromatography/mass spectrometry/mass spectrometry (LC/MS/MS). In addition, to determine whether renal LPA contributes to renal injury, we examined the effect of a LPA receptor antagonist on renal fibrosis following UUO in SD rats.

JPET Fast Forward. Published on December 4, 2020 as DOI: 10.1124/jpet.120.000353
This article has not been copyedited and formatted. The final version may differ from this version.

Materials and Methods

General.

Experiments were performed using male Sprague-Dawley (SD), Dahl salt-sensitive (Dahl S), and type 2 diabetic nephropathy (T2DN) rats. The SD rats were purchased from Charles River Laboratories (Wilmington, MA). The Dahl S and T2DN rats were obtained from inbred colonies maintained at the University of Mississippi Medical Center. The animals were housed in the Animal Care Facility at the University of Mississippi Medical Center that is approved by the American Association for the Accreditation of Laboratory Animal Care. The rats had free access to food and water throughout the study. Unless specifically mentioned, the rats were fed a normal rodent diet containing 1% NaCl (Harlan Teklad 8640; Harlan Laboratories, Madison, WI). All protocols were approved by the Institutional Animal Care and Use Committee of the University of Mississippi Medical Center.

Hypertensive model.

These experiments were performed on 12-week-old Dahl S rats maintained on a low salt (LS) diet containing 0.3% NaCl (Harlan Teklad 7034; Harlan Laboratories) from weaning. The rats were divided into two groups. One group was kept on a LS diet, while the other was switched to a high salt (HS) diet containing 8.0% NaCl (Harlan Teklad TD.92012; Harlan Laboratories). Blood pressure was measured using a tail-cuff device (Hatteras Instruments, Cary, NC). Twenty-four-hour urine samples were collected in metabolic cages to measure protein excretion. Urinary protein concentration was determined using the Bradford method (Bio-Rad Laboratories, Hercules, CA). At the end of the experiment, the kidneys were collected for measurement of LPA.

Diabetic models.

Nine-week-old Dahl S rats maintained on a normal salt diet containing 1% NaCl from weaning were treated with an intravenous injection of streptozotocin (STZ) (50 mg/kg,

JPET Fast Forward. Published on December 4, 2020 as DOI: 10.1124/jpet.120.000353
This article has not been copyedited and formatted. The final version may differ from this version.

Sigma-Aldrich, St. Louis, MO) to induce type 1 diabetes and a long-acting insulin implant was placed subcutaneously (2 U/day, Linshin Canada, ON, Canada) to maintain blood glucose levels around 400 mg/dl. Age-matched Dahl S rats served as non-diabetic controls. Four weeks after induction of diabetes, blood samples were collected from the tail vein for measurement of blood glucose and glycosylated hemoglobin (HbA1c). Urine samples were collected in metabolic cages to measure protein excretion. At the end of the experiment, the kidneys were collected for measurement of the LPA.

Six months (6M) and 18 months (18M) old T2DN rats were used as a model of type 2 diabetes that develops progressive proteinuria and diabetic nephropathy (Nobrega et al., 2004; Kojima et al., 2013a; Kojima et al., 2013b). Blood samples were collected for measurement of plasma glucose and HbA1c levels. Plasma glucose and HbA1c levels were measured using a glucometer (Bayer HealthCare, Mishawaka, IN) and a rapid HbA1c device (Bayer HealthCare, Sunnyvale, CA). Twenty-four-hour urine samples were collected via metabolic cages to study protein excretion, and the kidneys were collected for measurement of LPA.

Obstructive nephropathy model.

These experiments were performed on 7-week-old SD rats. The rats were anesthetized with isoflurane and placed on a heated surgical table to maintain body temperature at 37°C. A midline abdominal incision was made, and the left ureter was ligated at two points and cut between the ligatures. The abdominal incision was closed, and the rats were allowed to recover. Four days after ligation, the rats were anesthetized with isoflurane, and the left kidney was collected for measurement of LPA. Age-matched SD rats were studied as a control.

Measurement of renal LPA concentrations.

Samples of the renal cortex and outer medulla (approximately 20 mg) were homogenized in

JPET Fast Forward. Published on December 4, 2020 as DOI: 10.1124/jpet.120.000353
This article has not been copyedited and formatted. The final version may differ from this version.

1.2 mls of saline containing a phosphatase inhibitor cocktail (Calbiochem, San Diego, CA). The homogenate was transferred into a glass tube and acidified with acetic acid (Sigma-Aldrich) to pH 4. After the addition of 10 ng of 17:0 LPA (Avanti Polar Lipids, Alabaster, AL) as an internal standard, the samples were extracted with 1-butanol (EM Science, Cherry Hill, NJ). After centrifugation, the organic phase was transferred to a new glass tube. The aqueous phase was then re-extracted with water-saturated 1-butanol. The organic phase was combined with the initial fraction and dried under nitrogen. The extracted samples were analyzed by LC/MS/MS to determine the concentration of the various species of LPA, as described below.

LC/MS/MS analysis.

LPA standards, 16:0, 18:0 and 18:1 LPA, were purchased from Avanti Polar Lipids, Inc. (Alabaster, AL). Other standards, 18:2 and 20:4 LPA, were purchased from Echelon Biosciences Inc. (Salt Lake City, UT). The stock solutions of LPA standards and the internal standard, 17:0 LPA were prepared by dissolving the lipids in methanol and the stock solutions were stored at -20ºC. LPA was analyzed using a Dionex Ultimate 3000 LC system (Sunnyvale, CA) coupled to a QTRAP 4000 triple quadrupole-linear ion-trap mass spectrometer with a Turbo V ion-Source interface (AB Sciex, Foster City, CA). The samples were separated using an Atlantis T3 (3 μm), 2.1×75 mm analytical column proceeded by an Atlantis T3 (3 μm), 2.1×10 mm guard cartridge from Waters Corporation (Milford, MA). Mobile phase A (MP-A) contained 58% methanol, 41.8% water, 0.2% formic acid, and 5 mM ammonium formate. Mobile phase B (MP-B) consisted of 99% methanol, 0.8% water, 0.2% formic acid and 5 mM ammonium formate. The flow rate was set at 0.4 ml/min. The initial Mobile phase consisted of 25% MP-B for 1.5 min. The gradient was then ramped from 25% to 100% MP-B over 3.3 min and held there for 15.7 min. The MP was then returned to 25% MP-B for equilibration. The column oven

JPET Fast Forward. Published on December 4, 2020 as DOI: 10.1124/jpet.120.000353
This article has not been copyedited and formatted. The final version may differ from this version.

temperature was at 50ºC, and the autosampler temperature was maintained at 12ºC. The dried extracted samples were reconstituted in 200 μL of the mobile phase, and 10 μL were injected. For MS/MS analysis, a QTRAP 4000 triple quadrupole-linear ion trap mass spectrometer with a Turbo V ion-Source interface (AB Sciex, Foster City, CA) was operated in ESI negative ion multiple reaction monitoring (MRM) mode. The mass spectrometry parameters were for the LPAs were as follows: Ion Spray Voltage: -4,500V, Source Temperature: 400°C, Collision Gas: HIGH, Curtain Gas: 20 psi, Nebulizer Gas: 40 psi, and Heater Source Gas: 60 psi. For the MRM experiment of LPAs, the (M-1) - adduct ions were followed. Each LPA MRM parameters were optimized using direct infusions of standard LPAs (16:0, 18:0, 18:1, 18:2 and 20:4 LPA) in water-methanol-formic acid (1/1/0.1, v/v/v) solution. The MRMs followed (Q1 ion /Q3 fragment m/z pairs in parentheses) for each LPA species were: 16:0 (409.2/153), 18:0 (437.4/153), 18:1 (435.3/153), 18:2 (433.2/153), and 20:4 (457.2/153) and internal standard 17:0 (423.2/153). Values are expressed as the amount of the LPAs per gram of the tissue protein. The sum of all measured LPA species represents the total LPA tissue concentration.

Assay validation.

The linearity of the assay for each LPA species was assessed by analyzing the calibration curves. Calibration curves were generated by serial dilution into methanol over the range of 0.001 to 3 μM of each LPA species and 1 ng of the 17:0 LPA internal standard. The peak area ratio for each standard was calculated by dividing measured value by the peak area of 1 ng of the internal standard. The linearity of representative standard curves are presented in Supplemental Figure 1. Quality control (QC) samples were prepared by dissolving stock solution of LPA standards in saline at final concentrations of 0.4, 1, and 2 μM since a kidney matrix in the absence of LPA was not available. The intra- and inter-assay precisions were determined using the coefficients of variation, and the intra- and inter-assay

JPET Fast Forward. Published on December 4, 2020 as DOI: 10.1124/jpet.120.000353
This article has not been copyedited and formatted. The final version may differ from this version.

accuracies were defined as follows: (the measured values) / (the expected values) ×100. Intra-assay precision and accuracy were calculated using each concentration of the QC samples on the same day. Inter-assay accuracy and variations were calculated from measurements of the same standards over three separate days. Intra- and inter-assay precisions and accuracies for LPA species were shown in Supplemental Table 1.

Effect of Ki16425 on renal injury in obstructive nephropathy rats.

Vehicle (polyethylene glycol 400-corn oil-water, 1/1/0.5, v/v/v) or Ki16425 (100 mg/kg, NCE Biomedical, Wuhan, China) was administered subcutaneously twice daily for 7 consecutive days beginning on the day 1 of the UUO surgery. Ki16425 is reported to be a LPA_1 and LPA_3 antagonist (Ohta et al., 2003). Vehicle-treated sham-operated rats served as a control. Seven days after UUO, the rats were anesthetized with isoflurane, and the ligated kidney was collected for histological analysis. The kidneys were fixed in 10% formalin, and paraffin sections (3 μm) were prepared and stained with Masson's trichrome stain. Ten randomly chosen cortical and medullary fields (×100 total magnification) were captured using a Nikon Eclipse 55i microscope equipped with a Nikon DS-Fi1 color camera (Nikon Instruments Inc., Melville, NY). The degree of renal fibrosis was assessed by measuring the percentage of blue staining of collagen and fibronectin in the section using the NIS Elements D 3.0 software (Nikon Instruments Inc.).

Immunohistochemistry.

Kidneys were fixed in formalin, and 3 μm thick, paraffin sections were prepared and mounted on slides. The slides were deparaffinized in xylene, rehydrated through a decreasing ethanol gradient, and rinsed in PBS. The slides were pretreated with proteinase K (Dako, Carpinteria, CA) for 10 minutes and exposed to a blocking solution (Dako, Carpinteria, CA) for 30 minutes at room temperature. The slides were incubated with a monoclonal CD68 antibody (1:100; AbD Serotec, Raleigh, NC) overnight at 4°C, rinsed in

JPET Fast Forward. Published on December 4, 2020 as DOI: 10.1124/jpet.120.000353
This article has not been copyedited and formatted. The final version may differ from this version.

PBS, and then incubated with a secondary antibody conjugated with Alexa Fluor 488 (1:200; Jackson ImmunoResearch, West Grove, PA) for 1 hour. After three rinses in PBS, they were then counterstained with 0.001% Evans Blue (Sigma-Aldrich), rinsed in distilled water, and mounted with fluorescent mounting medium containing 4, 6-diamidino-2-phenylindole (Vector Laboratories, Burlingame, CA). Images were obtained using a Nikon Eclipse 55i microscope equipped with a 540-nm excitation filter and a 590-nm emission filter and a Nikon DS-Fi1 color camera.

Statistical analysis.

Data were presented as mean ± SEM. The significance of differences in mean values between two groups was determined using an unpaired t-test. The significance of the differences in mean values between multiple groups was determined using an ANOVA followed by a Holm-Sidak test for preplanned comparisons using the SigmaPlot 11 software (Systat Software, San Jose, CA).

JPET Fast Forward. Published on December 4, 2020 as DOI: 10.1124/jpet.120.000353
This article has not been copyedited and formatted. The final version may differ from this version.

Results

Blood pressure and renal injury in Dahl S rats fed a LS or HS diet.

A comparison of blood pressure and renal injury in Dahl S rats fed either a LS or HS diet for 4 weeks is presented in Table 1. Systolic blood pressure in Dahl S rats fed a HS diet was about 20 mmHg higher than the corresponding value measured in Dahl S rats fed a LS diet. The degree of proteinuria was 3-fold greater in Dahl S rats fed a HS diet than in Dahl S rats fed a LS diet.

Comparison of renal LPA levels in Dahl S rats fed a LS and HS diet.

A representative chromatogram showing the various LPA standards and a typical renal cortex LPA profile for Dahl S rats fed a LS or HS diet is presented in Figure 1. A comparison of the renal LPA levels in the renal cortex and outer medulla of the Dahl S rats fed either a LS or HS diet for 4 weeks is presented in Figure 2. The baseline levels of total LPA in the renal cortex and outer medulla of Dahl S rats fed a LS diet were above the normal level (Figure 2A, dashed line). The levels of total LPA in the renal cortex were significantly higher in Dahl S rats fed a HS diet than in those fed a LS diet (296.6 ± 22.9 versus 196.3 ± 8.5 nmol/g protein). In contrast, there were no significant differences in the total LPA levels in the renal outer medulla in Dahl S rats fed a LS or HS diet (Figure 2A). The most abundant LPA species in the renal cortex and outer medulla were 18:0, followed by 16:0 LPA (Figure 2B and 2C). The levels of 16:0 and 18:0 LPA in the renal cortex were significantly elevated in Dahl S rats fed a HS diet in comparison to those fed a LS diet (Figure 2B).

Blood glucose and renal injury in control and STZ induced diabetic Dahl S rats.

A comparison of blood glucose and renal injury in control and STZ induced diabetic Dahl S

JPET Fast Forward. Published on December 4, 2020 as DOI: 10.1124/jpet.120.000353
This article has not been copyedited and formatted. The final version may differ from this version.

rats is presented in Table 2. After 4 weeks of STZ injection, blood glucose levels (485.4 ± 62.3 versus 88.0 ± 10.5 mg/dl) and HbA1c concentrations (11.5 ± 0.6 versus 4.9 ± 0.2%) were significantly elevated in STZ-induced diabetic Dahl S rats in comparison to control Dahl S rats. Urine output in STZ-induced diabetic Dahl S rats was significantly higher than the corresponding value measured in control Dahl S rats. The degree of proteinuria was 4-fold greater in STZ-treated diabetic Dahl S rats than control rats.

Comparison of renal LPA levels in control and STZ induced diabetic Dahl S rats.

A comparison of the renal LPA levels in the renal cortex and outer medulla of control and STZ-treated diabetic Dahl S rats is presented in Figure 3. There were no differences in the total LPA levels in the renal cortex in control and STZ-induced diabetic Dahl S rats (Figure 3A). The total LPA levels in the renal outer medulla were markedly increased in STZ-induced diabetic Dahl S rats in comparison to control rats (624.6 ± 129.5 versus 318.8 ± 17.1 nmol/g protein), mainly due to an elevation in 18:0 LPA (Figure 3A and 3C). Saturated LPAs (16:0 and 18:0 LPA) were the predominant species in the renal cortex and outer medulla of control and STZ-induced diabetic Dahl S rats (Figure 3B and 3C). The level of 18:0 LPA in renal outer medulla was significantly increased in STZ-induced diabetic Dahl S rats compared with that seen in control Dahl S rats (Figure 3C).

Blood glucose and renal injury in 6M and 18M old T2DN rats.

A comparison of blood glucose concentration and proteinuria in 6M and 18M old T2DN rats is presented in Table 3. Both 6M and 18M old T2DN rats were diabetic, and blood glucose and HbA1c levels were elevated to >200 mg/dl and >8%, respectively. Proteinuria was 6-fold greater in 18M old T2DN rats than 6M old T2DN rats (325.0 ± 35.5 versus 55.5 ± 15.8 mg/day).

JPET Fast Forward. Published on December 4, 2020 as DOI: 10.1124/jpet.120.000353
This article has not been copyedited and formatted. The final version may differ from this version.

Comparison of renal LPA levels in 6M and 18M old T2DN rats.

A comparison of the renal LPA levels in the renal cortex and outer medulla of 6M and 18M old T2DN rats is presented in Figure 4. The total LPA levels in the renal cortex were significantly higher in 18M old T2DN rats than in 6M old T2DN rats (184.9 ± 20.9 versus 116.9 ± 6.0 nmol/g protein). There were no significant differences in the total LPA levels in the renal outer medulla between the 6M and 18M old T2DN rats (Figure 4A). The most abundant LPA species in the renal cortex and outer medulla of the 6M and 18M old T2DN rats were 18:0, followed by 20:4 LPA (Figure 4B and 4C). There was a major elevation in 18:0 LPA levels in the renal cortex, and lesser increases in 16:0, 18:1, and 18:2 LPA in the 18M old T2DN rats.

Comparison of renal LPA levels in control and UUO SD rats.

A comparison of renal LPA levels in the renal cortex and outer medulla in control and UUO SD rats is presented in Figure 5. The levels of total LPA in the renal cortex were significantly higher in UUO than in control SD rats. In contrast, there were no significant differences in the total LPA levels in the renal outer medulla of control and UUO SD rats (Figure 5A). The most abundant LPA species in the renal cortex and outer medulla of the control and UUO SD rats were 18:0 LPA, followed by 16:0 and 20:4 LPA (Figure 5B and 5C). The levels of 16:0, 18:0, 18:1, and 18:2 LPA were significantly elevated in the renal cortex of UUO in comparison to control SD rats (Figure 5B). The levels of 18:2 and 20:4 LPA in renal outer medulla were also significantly higher in UUO than in control SD rats (Figure 5C).

Effects of Ki16425 on renal injury in UUO rats.

JPET Fast Forward. Published on December 4, 2020 as DOI: 10.1124/jpet.120.000353
This article has not been copyedited and formatted. The final version may differ from this version.

To examine whether elevated renal LPA levels contribute to renal injury, we studied the effect of LPA receptor antagonist, Ki16425, on renal fibrosis in UUO rats. The effects of Ki16425 on renal fibrosis in UUO rats are presented in Figure 6. The degree of fibrosis in the renal cortex and medulla were greater in the vehicle-treated UUO than in sham-operated rats (Figure 6A). The percentage of cortical (Figure 6B) and medullary (Figure 6C) areas stained with Mason's trichrome were 4- and 12-fold greater in vehicle-treated UUO than in sham-operated rats. Chronic treatment with Ki16425 markedly reduced cortical and medullary fibrosis by 66 and 32%, respectively, compared with the levels measured in vehicle-treated UUO rats. We also examined immune cell infiltration in the kidney of UUO rats. The number of CD68 positive immune cells in the cortical region was significantly higher in the vehicle-treated UUO than in sham-operated rats (Figure 7). Treatment with Ki16425 significantly decreased the number of CD68 positive cells in the kidney of UUO rats.

JPET Fast Forward. Published on December 4, 2020 as DOI: 10.1124/jpet.120.000353
This article has not been copyedited and formatted. The final version may differ from this version.

Discussion

The present study determined whether the renal LPA levels increase during the development of renal injury in rat models of hypertension, diabetes, and obstructive nephropathy, using LC/MS/MS. Additionally, the possible role of renal LPA in renal fibrosis was investigated in UUO rats using a LPA receptor antagonist. The Dahl S rat is a well-established genetic model of salt-sensitive hypertension that rapidly develops severe progressive proteinuria, glomerulosclerosis, interstitial fibrosis and a decline in GFR when fed a HS diet (Chen et al., 1993; Dahly et al., 2002; Dahly-Vernon et al., 2005). The present results indicate that Dahl S rats fed a HS diet developed hypertension and renal injury, as indicated by an elevation in blood pressure and proteinuria as compared to Dahl S rats maintained on a LS diet. We found that total LPA levels increased to a much greater extent in the renal cortex of Dahl S rats fed a HS diet than that seen in Dahl S rats fed a LS diet. These findings suggest that elevated levels of LPA may contribute to the development of hypertension-related renal injury in Dahl S rats. We also found that the baseline levels of total LPA were higher in control Dahl S rats fed a normal salt diet in the diabetic studies than those seen in Dahl S rats fed a LS diet. Although it is possible that moderate increases in salt intake may directly affect renal LPA levels, a more likely explanation is that the difference reflects the degree of renal injury and inflammation since Dahl S rats develop more hypertension and proteinuria with age when maintained on a normal versus LS diet (McPherson et al., 2020; Chen et al., 2013).

We next evaluated the renal LPA levels in type 1 and 2 models of diabetic nephropathy. STZ-induced diabetic Dahl S rat is a type 1 diabetic model that has been reported to develops the all the features of diabetic nephropathy including; hyperfiltration, thickening of basement membranes, mesangial matrix expansion, progressive proteinuria, glomerulosclerosis, interstitial fibrosis, and more than a 50% decline in GFR (Slaughter et

al., 2013; Kojima et al., 2015). We found that blood glucose, HbA1c, and proteinuria were significantly higher in STZ-induced diabetic Dahl S rats compared with age-matched controls. LPA levels increased significantly in the renal outer medulla of STZ-induced diabetic Dahl S rats in comparison to the levels seen in age-matched controls.

The T2DN rat is a genetic model of diabetic nephropathy that was created by introducing the mitochondrial genome of the Fawn Hooded Hypertensive rat into the genetic background of the Goto-Kakizaki rat that develops type 2 diabetes but not progressive renal disease. Previous studies have indicated that T2DN rats develop diabetes at 3 months of age, and diabetic nephropathy, including thickening of glomerular basement membrane, focal glomerulosclerosis, interstitial fibrosis, and a fall in GFR as they increase in age from 6 to 18 months. (Kojima et al., 2013a, b). The results of the present study indicated that LPA levels were elevated in the renal cortex of 18M old T2DN rats with more severe renal injury than in 6M old T2DN rats. These findings suggest that elevations in renal LPA may contribute to the development of renal injury associated with both type 1 and 2 models of diabetic nephropathy. The differences between the two models were that LPA levels increased in the renal outer medulla in STZ-induced diabetic Dahl S rats, whereas LPA levels increased in the renal cortex in the 18M old T2DN rats. STZ-induced diabetic Dahl S rat is an accelerated type 1 diabetic model which develops renal injury and decline in GFR over a span of 12 weeks, whereas the T2DN rat is a genetic model of type 2 diabetes that slowly develops CKD between 12 and 18M of age. Although the reason for the difference remains to be determined, one possible explanation for the differences may be due to either the type of diabetes or the progression of diabetic nephropathy.

We also examined the renal LPA levels in UUO rats, which is an animal model typically used to study renal fibrosis, inflammation, and extracellular matrix accumulation. The present results indicate that total LPA levels were elevated in the renal cortex of UUO

rats compared with control SD rats. These results are consistent with the previous findings that the release of LPA increased in the kidney explants isolated from UUO mice (Pradère et al., 2007). Taken together, the present results suggest that the formation and/or the release of LPA increases in the kidney during the development of renal injury. Consistent with this suggestion, previous investigators reported that the levels of LPA were elevated in the renal effluent collected from the pelvis of UUO rats, and this was associated with an increase in the renal expression of LPA-producing enzymes, acylglycerol kinase and autotaxin (Tsutsumi et al., 2011). Moreover, the expression of autotaxin has been reported to be elevated in the kidney of diabetic patients and animal models of diabetic nephropathy (Zhang et al., 2017).

In the setting of renal injury, LPA may exert a host of biological effects on a variety of renal cell types, including proximal tubular cells, mesangial cells, and fibroblasts (Inoue et al., 1997; Fang et al., 2000; Geng et al., 2012). Recently, LPA has been implicated in the pathogenesis of tissue fibrosis in the lung, liver, and kidney (Pradère et al., 2008; Ikeda and Yatomi, 2012; Shea and Tager, 2012). Renal fibrosis is a final common pathway underlying the progression of CKD to ESRD (Hodgkins and Schnaper, 2012). Previous studies indicated that there were no significant changes in plasma LPA levels in UUO rats (Tsutsumi et al., 2011). Therefore, to examine whether the elevation of renal LPA contributes to renal injury, we studied the effect of LPA receptor antagonist, Ki16425, on renal fibrosis in UUO rats. We found that Ki16425 attenuated the progression of renal fibrosis and CD68 positive immune cell infiltration following UUO, suggesting that increases in renal LPA may, at least in part, contribute to the renal inflammation and fibrosis in UUO rats. UUO model reflects important aspects of renal inflammation and fibrosis that are prominent feature of CKD. However, UUO model lacks the functional readouts of CKD, in that serum creatinine levels are normal and there is little if any

proteinuria because contralateral non-obstructed kidney is normal and injured kidney has no urine output. Therefore, additional future studies will be needed to determine whether Ki16425 has the potential to improve renal function in chronic models of hypertension induced CKD or diabetic nephropathy.

The origin of renal LPA and the species formed is not well understood. This is the first study to profile the formation of various species of LPA in the renal cortex and outer medulla in various models of renal disease. The results indicate that the most dominant species of LPA found in the renal cortex, and outer medulla was 18:0 LPA in all of the disease models studied. This finding is in line with previous studies that the predominant LPA species in renal effluent of UUO rats was 18:0 LPA (Tsutsumi et al., 2011). On the other hand, several studies indicate that the predominant LPA species that circulate in the plasma of rats are the unsaturated LPA species: 18:2 and 20:4 LPA (Saga et al., 2014; Ino et al., 2012). These findings, together with our new results, suggest that elevations of renal LPA levels are due to local LPA production in the kidney rather filtration and uptake of LPA from the plasma since the composition of LPA species in the kidney and plasma are markedly different.

Previous studies have indicated that LPA species that differ in the length and degree of saturation of the fatty acyl chain have distinct biological effects (Bandoh et al., 2000; Yoshida et al., 2003). In this study, we found that saturated LPAs were the species that were increased in the kidney of rats with renal disease. Although it is unclear that how signaling of saturated LPA species differs from that of unsaturated species, our findings suggest that one should focus on signaling pathways and receptors that medicate the responses to saturated LPAs in the search for new potential therapeutics to prevent renal disease. In contrast, previous studies indicated that LPA receptors have a relatively higher affinity for unsaturated LPA species than for saturated species (Tigyi, 2010). Therefore,

JPET Fast Forward. Published on December 4, 2020 as DOI: 10.1124/jpet.120.000353
This article has not been copyedited and formatted. The final version may differ from this version.

further studies are needed to determine the significance of elevation of saturated LPA species in renal disease.

In summary, the present study indicates that the renal formation of LPA, especially saturated species, increase during the development of renal injury in rat models of hypertension, diabetes, and following obstructive nephropathy. In addition, administration of a LPA receptor antagonist attenuated the progression of renal injury in UUO rat model of renal fibrosis. These results suggest that the increases in renal LPA production may contribute to the pathophysiology of CKD, and that therapeutic approaches that target the renal formation of LPA or block the LPA receptor might be renoprotective and have therapeutic potential.

JPET Fast Forward. Published on December 4, 2020 as DOI: 10.1124/jpet.120.000353
This article has not been copyedited and formatted. The final version may differ from this version.

Acknowledgment

The authors thank Dr. Naoki Kojima and Dr. Yoshikazu Muroya for their assistance and helpful comments for this project. The authors thank Christine A. Purser for the LC/MS/MS analysis.

JPET Fast Forward. Published on December 4, 2020 as DOI: 10.1124/jpet.120.000353
This article has not been copyedited and formatted. The final version may differ from this version.

Authorship Contributions

Participated in research design: Hirata, Smith, Takahashi, Miyata, and Roman

Conducted experiments: Hirata

Performed data analysis: Hirata and Roman

Wrote or contributed to the writing of the manuscript: Hirata and Roman

JPET Fast Forward. Published on December 4, 2020 as DOI: 10.1124/jpet.120.000353
This article has not been copyedited and formatted. The final version may differ from this version.

References

Aikawa S, Hashimoto T, Kano K, Aoki J (2015) Lysophosphatidic acid as a lipid mediator with multiple biological actions. *J Biochem* **157:** 81-89.

Aoki J, Inoue A, Okudaira S (2008) Two pathways for lysophosphatidic acid production. *Biochim Biophys Acta* **1781:** 513-518.

Bandoh K, Aoki J, Taira A, Tsujimoto M, Arai H, Inoue K (2000) Lysophosphatidic acid (LPA) receptors of the EDG family are differentially activated by LPA species. Structure-activity relationship of cloned LPA receptors. *FEBS Lett* **478:** 159-165.

Benesch MG, Tang X, Venkatraman G, Bekele RT, Brindley DN (2016) Recent advances in targeting the autotaxin-lysophosphatidate-lipid phosphate phosphatase axis in vivo. *J Biomed Res* **30:** 272-284.

Chen CC, Geurts AM, Jacob HJ, Fan F, Roman RJ (2013) Heterozygous knockout of transforming growth factor-β1 protects Dahl S rats against high salt-induced renal injury. *Physiol Genomics* **45:** 110-118.

Chen PY, St John PL, Kirk KA, Abrahamson DR, Sanders PW (1993) Hypertensive nephrosclerosis in the Dahl/Rapp rat. Initial sites of injury and effect of dietary L-arginine supplementation. *Lab Invest* **68:** 174-184.

Dahly AJ, Hoagland KM, Flasch AK, Jha S, Ledbetter SR, Roman RJ (2002) Antihypertensive effects of chronic anti-TGF-β antibody therapy in Dahl S rats. *Am J Physiol Regul Integr Comp Physiol* **283:** R757-R767.

Dahly-Vernon AJ, Sharma M, McCarthy ET, Savin VJ, Ledbetter SR, Roman RJ (2005) Transforming growth factor-β, 20-HETE interaction, and glomerular injury in Dahl salt-sensitive rats. *Hypertension* **45:** 643-648.

Dohi T, Miyauchi K, Ohkawa R, Nakamura K, Kishimoto T, Miyazaki T, Nishino A, Nakajima N, Yaginuma K, Tamura H, Kojima T, Yokoyama K, Kurata T, Shimada K,

Yatomi Y, Daida H (2012) Increased circulating plasma lysophosphatidic acid in patients with acute coronary syndrome. *Clin Chim Acta* **413:** 207-212.

Eichholtz T, Jalink K, Fahrenfort I, Moolenaar WH (1993) The bioactive phospholipid lysophosphatidic acid is released from activated platelets. *Biochem J* **291:** 677-680.

Fang X1, Yu S, LaPushin R, Lu Y, Furui T, Penn LZ, Stokoe D, Erickson JR, Bast RC Jr, Mills GB (2000) Lysophosphatidic acid prevents apoptosis in fibroblasts via G(i)-protein-mediated activation of mitogen-activated protein kinase. *Biochem J* **352:** 135-143.

Gansevoort RT, Correa-Rotter R, Hemmelgarn BR, Jafar TH, Heerspink HJ, Mann JF, Matsushita K, Wen CP (2013) Chronic kidney disease and cardiovascular risk: epidemiology, mechanisms, and prevention. *Lancet* **382:** 339-352.

Geng H, Lan R, Singha PK, Gilchrist A, Weinreb PH, Violette SM, Weinberg JM, Saikumar P, Venkatachalam MA (2012) Lysophosphatidic acid increases proximal tubule cell secretion of profibrotic cytokines PDGF-B and CTGF through LPA_2- and Gαq-mediated Rho and αvβ6 integrin-dependent activation of TGF-β. *Am J Pathol* **181:** 1236-1249.

Grove KJ, Voziyan PA, Spraggins JM, Wang S, Paueksakon P, Harris RC, Hudson BG, Caprioli RM (2014) Diabetic nephropathy induces alterations in the glomerular and tubule lipid profiles. *J Lipid Res* **55:** 1375-1385.

Hayashi K, Takahashi M, Nishida W, Yoshida K, Ohkawa Y, Kitabatake A, Aoki J, Arai H, Sobue K (2001) Phenotypic modulation of vascular smooth muscle cells induced by unsaturated lysophosphatidic acids. *Circ Res* **89:** 251-258.

Hodgkins KS, Schnaper HW (2012) Tubulointerstitial injury and the progression of chronic kidney disease. *Pediatr Nephrol* **27:** 901-909.

Ikeda H, Yatomi Y (2012) Autotaxin in liver fibrosis. *Clin Chim Acta* **413:** 1817-1821.

Ino M, Shimizu Y, Tanaka T, Tokumura A (2012) Alterations of plasma levels of lysophosphatidic acid in response to fasting of rats. *Biol Pharm Bull* **35:** 2059-2063.

Inoue CN, Epstein M, Forster HG, Hotta O, Kondo Y, Iinuma K (1999) Lysophosphatidic acid and mesangial cells: implications for renal diseases. *Clin Sci (Lond)* **96:** 431-436.

Inoue CN, Forster HG, Epstein M (1995) Effects of lysophosphatidic acid, a novel lipid mediator, on cytosolic Ca2+ and contractility in cultured rat mesangial cells. *Circ Res* **77:** 888-896.

Inoue CN, Ko YH, Guggino WB, Forster HG, Epstein M (1997) Lysophosphatidic acid and platelet-derived growth factor synergistically stimulate growth of cultured rat mesangial cells. *Proc Soc Exp Biol Med* **216:** 370-379.

Kojima N, Slaughter TN, Paige A, Kato S, Roman RJ, Williams JM (2013a) Comparison of the Development Diabetic Induced Renal Disease in Strains of Goto-Kakizaki Rats. *J Diabetes Metab Suppl* **9:** S9-005.

Kojima N, Williams JM, Slaughter TN, Kato S, Takahashi T, Miyata N, Roman RJ (2015) Renoprotective effects of combined SGLT2 and ACE inhibitor therapy in diabetic Dahl S rats. *Physiol Rep* **3:** e12436.

Kojima N, Williams JM, Takahashi T, Miyata N, Roman RJ (2013b) Effects of a new SGLT2 inhibitor, luseogliflozin, on diabetic nephropathy in T2DN rats. *J Pharmacol Exp Ther* **345:** 464-472.

McPherson KC, Shields CA, Poudel B, Johnson AC, Taylor L, Stubbs C, Nichols A, Cornelius DC, Garrett MR, Williams JM (2020) Altered renal hemodynamics is associated with glomerular lipid accumulation in obese Dahl salt-sensitive leptin receptor mutant rats. *Am J Physiol Renal Physiol* **318:** F911-F921.

Meleh M, Pozlep B, Mlakar A, Meden-Vrtovec H, Zupancic-Kralj L (2007) Determination

of serum lysophosphatidic acid as a potential biomarker for ovarian cancer. *J Chromatogr B Analyt Technol Biomed Life Sci* **858:** 287-291.

Mirzoyan K, Baïotto A, Dupuy A, Marsal D, Denis C, Vinel C, Sicard P, Bertrand-Michel J, Bascands JL, Schanstra JP, Klein J, Saulnier-Blache JS (2016) Increased urinary lysophosphatidic acid in mouse with subtotal nephrectomy: potential involvement in chronic kidney disease. *J Physiol Biochem* **72:** 803-812.

Mutoh T, Rivera R, Chun J (2012) Insights into the pharmacological relevance of lysophospholipid receptors. *Br J Pharmacol* **165:** 829-844.

Nakanaga K, Hama K, Aoki J (2010) Autotaxin--an LPA producing enzyme with diverse functions. *J Biochem* **148:** 13-24.

Nobrega MA, Fleming S, Roman RJ, Shiozawa M, Schlick N, Lazar J, Jacob HJ (2004) Initial characterization of a rat model of diabetic nephropathy. *Diabetes* **53:** 735-742.

Ohta H, Sato K, Murata N, Damirin A, Malchinkhuu E, Kon J, Kimura T, Tobo M, Yamazaki Y, Watanabe T, Yagi M, Sato M, Suzuki R, Murooka H, Sakai T, Nishitoba T, Im DS, Nochi H, Tamoto K, Tomura H, Okajima F (2003) Ki16425, a subtype-selective antagonist for EDG-family lysophosphatidic acid receptors. *Mol Pharmacol* **64:** 994-1005.

Pradère JP, Gonzalez J, Klein J, Valet P, Grès S, Salant D, Bascands JL, Saulnier-Blache JS, Schanstra JP (2008) Lysophosphatidic acid and renal fibrosis. *Biochim Biophys Acta* **1781:** 582-587.

Pradère JP, Klein J, Grès S, Guigné C, Neau E, Valet P, Calise D, Chun J, Bascands JL, Saulnier-Blache JS, Schanstra JP (2007) LPA_1 receptor activation promotes renal interstitial fibrosis. *J Am Soc Nephrol* **18:** 3110-3118.

Saga H, Ohhata A, Hayashi A, Katoh M, Maeda T, Mizuno H, Takada Y, Komichi Y, Ota H, Matsumura N, Shibaya M, Sugiyama T, Nakade S, Kishikawa K (2014) A novel

highly potent autotaxin/ENPP2 inhibitor produces prolonged decreases in plasma lysophosphatidic acid formation in vivo and regulates urethral tension. *PLoS One* **9:** e93230.

Saulnier-Blache JS, Feigerlova E, Halimi JM, Gourdy P, Roussel R, Guerci B, Dupuy A, Bertrand-Michel J, Bascands JL, Hadjadj S, Schanstra JP (2017) Urinary lysophopholipids are increased in diabetic patients with nephropathy. *J Diabetes Complications* **31:** 1103-1108.

Sharma S, Sarnak MJ (2017) Epidemiology: The global burden of reduced GFR: ESRD, CVD and mortality. *Nat Rev Nephrol* **13:** 447-448.

Shea BS, Tager AM (2012) Role of the lysophospholipid mediators lysophosphatidic acid and sphingosine 1-phosphate in lung fibrosis. *Proc Am Thorac Soc* **9:** 102-110.

Slaughter TN, Paige A, Spires D, Kojima N, Kyle PB, Garrett MR, Roman RJ, Williams JM (2013) Characterization of the development of renal injury in Type-1 diabetic Dahl salt-sensitive rats. *Am J Physiol Regul Integr Comp Physiol* **305:** R727-R734.

Swaney JS, Chapman C, Correa LD, Stebbins KJ, Broadhead AR, Bain G, Santini AM, Darlington J, King CD, Baccei CS, Lee C, Parr TA, Roppe JR, Seiders TJ, Ziff J, Prasit P, Hutchinson JH, Evans JF, Lorrain DS (2011) Pharmacokinetic and pharmacodynamic characterization of an oral lysophosphatidic acid type 1 receptor-selective antagonist. *J Pharmacol Exp Ther* **336:** 693-700.

Tigyi G (2010) Aiming drug discovery at lysophosphatidic acid targets. *Br J Pharmacol* **161:** 241-270.

Tonelli M Wiebe N, Culleton B, House A, Rabbat C, Fok M, McAlister F, Garg AX (2006) Chronic kidney disease and mortality risk: a systematic review. *J Am Soc Nephrol* **17:** 2034-2047.

Tsutsumi T, Adachi M, Nikawadori M, Morishige J, Tokumura A (2011) Presence of

bioactive lysophosphatidic acid in renal effluent of rats with unilateral ureteral obstruction. *Life Sci* **89:** 195-203.

Xie Y, Bowe B, Mokdad AH, Xian H, Yan Y, Li T, Maddukuri G, Tsai CY, Floyd T. Al-Aly Z (2018) Analysis of the Global Burden of Disease study highlights the global, regional, and national trends of chronic kidney disease epidemiology from 1990 to 2016. *Kidney Int* **94:** 567-581.

Yoshida K, Nishida W, Hayashi K, Ohkawa Y, Ogawa A, Aoki J, Arai H, Sobue K (2003) Vascular remodeling induced by naturally occurring unsaturated lysophosphatidic acid in vivo. *Circulation* **108:** 1746-1752.

Zhang MZ, Wang X, Yang H, Fogo AB, Murphy BJ, Kaltenbach R, Cheng P, Zinker B, Harris RC (2017) Lysophosphatidic Acid Receptor Antagonism Protects against Diabetic Nephropathy in a Type 2 Diabetic Model. *J Am Soc Nephrol* **28:** 3300-3311.

JPET Fast Forward. Published on December 4, 2020 as DOI: 10.1124/jpet.120.000353
This article has not been copyedited and formatted. The final version may differ from this version.

Footnotes

T.H., T.T. and N.M. are employees of Taisho Pharmaceutical Co., Ltd. that develops drugs for a wide range of diseases, including cardiovascular diseases. R.J.R. and S.V.S. are employees of the University of Mississippi Medical Center, and receive funding from the National Institutes of Health to explore the genetic basis of renal and cerebrovascular disease. This work was partially supported by funds provided by Taisho Pharmaceutical Co., Ltd., Saitama, Japan and grants R01 HL36279 and DK104184 from the National Institutes of Health.

JPET Fast Forward. Published on December 4, 2020 as DOI: 10.1124/jpet.120.000353
This article has not been copyedited and formatted. The final version may differ from this version.

Figure Legends

Figure 1. LC/MS separation and peak height comparisons after 1 ng injections of various LPA standards (A). 18:2 (dashed line) and 20:4 LPAs that overlap in retention time were distinguishable based on their unique MRMs (433.2/153 and 457/153; respectively) (A). Comparison of a typical LPA profiles of extracts of the renal cortex of Dahl S rats fed a low salt (LS) or high salt (HS) diet (B).

Figure 2. Comparison of renal LPA levels in Dahl S rats fed a low salt (LS) or high salt (HS) diet for 4 weeks. Total LPA levels in renal cortex and outer medulla (A). The molecular species composition of LPA in renal cortex (B) and outer medulla (C). Mean values ± SEM are presented. Numbers in parentheses indicate the number of rats studied per group. For comparison, the dashed line represents the total LPA levels measured in the kidneys of control SD rats fed a normal salt diet. The SD data is replotted from Figure 5. *: $P<0.05$ vs. the corresponding value measured in Dahl S rats fed a LS diet.

Figure 3. Comparison of renal LPA levels in control and STZ induced diabetic Dahl S rats. Total LPA levels in renal cortex and outer medulla (A). The molecular species composition of LPA in renal cortex (B) and outer medulla (C). Mean values ± SEM are presented. Numbers in parentheses indicate the number of rats studied per group. *: $P<0.05$ vs. the corresponding value measured in control Dahl S rats.

Figure 4. Comparison of renal LPA levels in 6-month (6M) and 18-month (18M) old T2DN rats. Total LPA levels in renal cortex and outer medulla (A). The molecular species composition of LPA in renal cortex (B) and outer medulla (C). Mean values ± SEM are presented. Numbers in parentheses indicate the number of rats studied per group. *: $P<0.05$

JPET Fast Forward. Published on December 4, 2020 as DOI: 10.1124/jpet.120.000353
This article has not been copyedited and formatted. The final version may differ from this version.

vs. the corresponding value measured in 6M old T2DN rats.

Figure 5. Comparison of renal LPA levels in control and UUO SD rats. Total LPA levels in renal cortex and outer medulla (A). The molecular species composition of LPA in renal cortex (B) and outer medulla (C). Mean values ± SEM are presented. Numbers in parentheses indicate the number of rats studied per group. *: P<0.05 vs. the corresponding value measured in control SD rats.

Figure 6. Effects of Ki16425 (200 mg/kg/day) on renal fibrosis in UUO rats. Representative images of the renal cortex and medulla stained with Masson's trichrome in sham and UUO rats treated with vehicle or Ki16425 (A). Quantitative analysis of blue staining area was performed on 10 random non-overlapping fields in the renal cortex (B) and medulla (C). Magnification is 100X. Mean values ± SEM are presented. Numbers in parentheses indicate the number of areas scored and the number of rats studied per group *: P<0.05 vs. the corresponding value measured in sham rats. †: P<0.05 vs. the corresponding value measured in vehicle-treated UUO rats.

Figure 7. Effects of Ki16425 on immune cells infiltration in UUO rats. Representative images of the renal cortex were stained with CD68 antibody (green) in sham and UUO rats treated with vehicle or Ki16425. The tissues were counterstained with DAPI to visualize nuclei (blue) and 0.001% Evans blue (red) to quench green autofluorescence and visualize tubular structure. The number of CD68 positive immune cells in the renal cortex was counted in 10 random non-overlapping fields per rat. Magnification is 200X. Mean values ± SEM are presented. Numbers in parentheses indicate the number of areas scored and the number of rats studied per group. *: P<0.05 vs. the corresponding value measured in sham

JPET Fast Forward. Published on December 4, 2020 as DOI: 10.1124/jpet.120.000353
This article has not been copyedited and formatted. The final version may differ from this version.

rats. †: P<0.05 vs. the corresponding value measured in vehicle-treated UUO rats.

JPET Fast Forward. Published on December 4, 2020 as DOI: 10.1124/jpet.120.000353
This article has not been copyedited and formatted. The final version may differ from this version.

Tables

TABLE 1

Metabolic parameters of Dahl S rats fed a low salt (LS) or high salt (HS) diet.

	Dahl-LS (5)			Dahl-HS (5)		
Body Weight, g	390.4	±	10.9	355.0	±	3.9*
Kidney Weight, g	1.23	±	0.05	1.54	±	0.04*
Systolic Blood Pressure, mmHg	182.6	±	3.9	202.9	±	5.6*
Urine Flow Rate, ml/day	22.2	±	8.0	97.2	±	3.9*
Proteinuria, mg/day	120.8	±	22.0	330.6	±	66.9*

Mean values ± SEM are presented.

Numbers in parentheses indicate the number of rats studied per group.

*$p<0.05$ vs. corresponding values measured in Dahl S rats fed a LS diet.

JPET Fast Forward. Published on December 4, 2020 as DOI: 10.1124/jpet.120.000353
This article has not been copyedited and formatted. The final version may differ from this version.

TABLE 2.

Metabolic parameters of control and STZ-treated diabetic Dahl S (Dahl-STZ) rats.

	Dahl S (5)			Dahl-STZ (5)		
Body Weight, g	398.6	±	20.8	337.4	±	16.6
Kidney Weight, g	1.32	±	0.08	1.81	±	0.06*
Blood Glucose, mg/dl	88.0	±	10.5	485.4	±	62.3*
HbA1c, %	4.9	±	0.2	11.5	±	0.6*
Urine Flow Rate, ml/day	7.4	±	0.9	101.6	±	9.1*
Proteinuria, mg/day	126.2	±	18.4	495.3	±	65.4*

Mean values ± SEM are presented.

Numbers in parentheses indicate the number of rats studied per group.

*$p<0.05$ vs. corresponding values measured in control Dahl S rats.

JPET Fast Forward. Published on December 4, 2020 as DOI: 10.1124/jpet.120.000353
This article has not been copyedited and formatted. The final version may differ from this version.

TABLE 3.

Metabolic parameters of 6-month (6M) and 18-month (18M) old T2DN rats.

	6M T2DN (5)			18M T2DN (10)		
Body Weight, g	388.4	±	13.5	429.3	±	11.2*
Kidney Weight, g	1.42	±	0.05	1.91	±	0.08*
Blood Glucose, mg/dl	367.6	±	61.4	216.2	±	21.9*
HbA1c, %	10.4	±	1.0	8.1	±	0.5*
Urine Flow Rate, ml/day	41.0	±	15.4	34.6	±	5.0
Proteinuria, mg/day	55.5	±	15.8	325.0	±	35.5*

Mean values ± SEM are presented.

Numbers in parentheses indicate the number of rats studied per group.

*$p<0.05$ vs. corresponding values measured in 6M old T2DN rats.

JPET Fast Forward. Published on December 4, 2020 as DOI: 10.1124/jpet.120.000353
This article has not been copyedited and formatted. The final version may differ from this version.

Figure 1

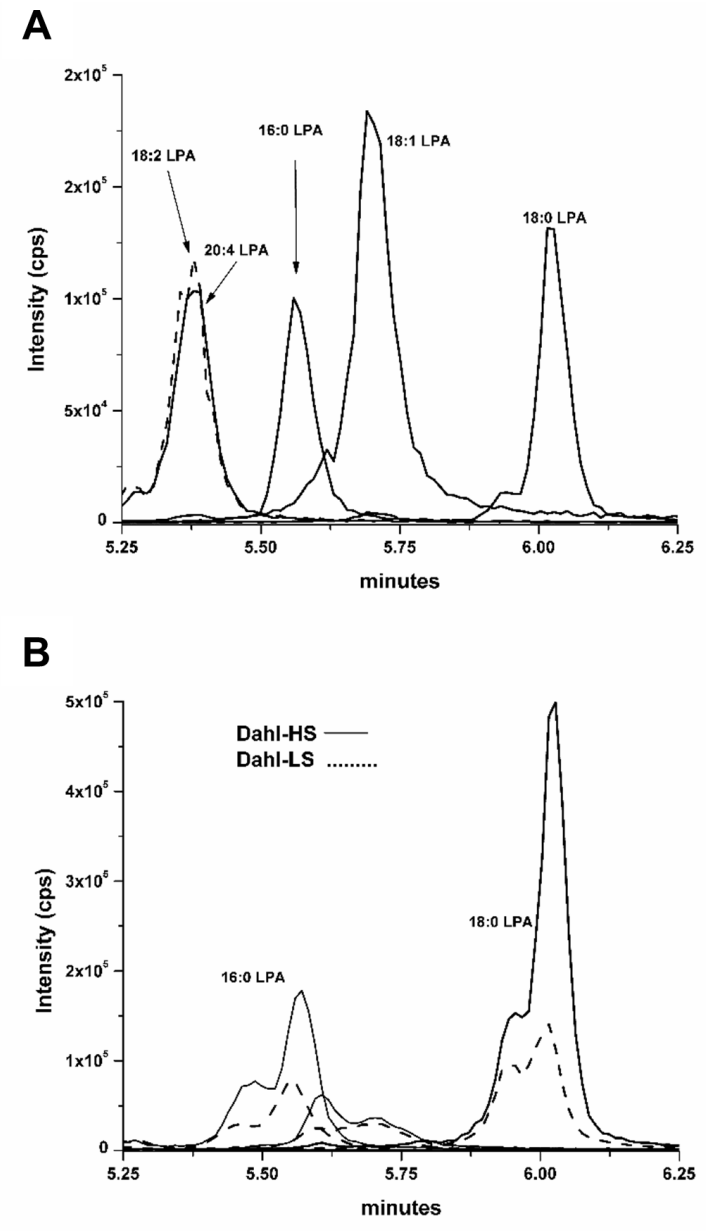

JPET Fast Forward. Published on December 4, 2020 as DOI: 10.1124/jpet.120.000353
This article has not been copyedited and formatted. The final version may differ from this version.

Figure 2

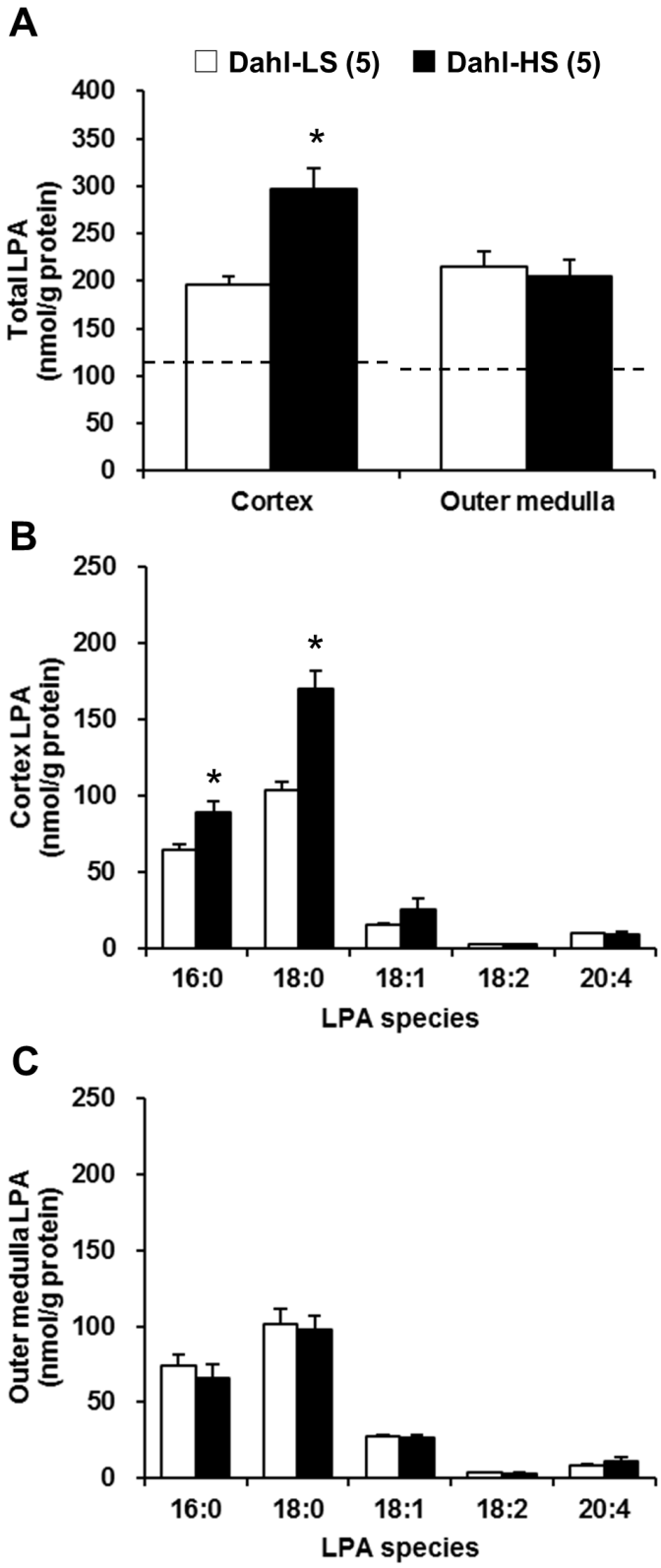

JPET Fast Forward. Published on December 4, 2020 as DOI: 10.1124/jpet.120.000353
This article has not been copyedited and formatted. The final version may differ from this version.

Figure 3

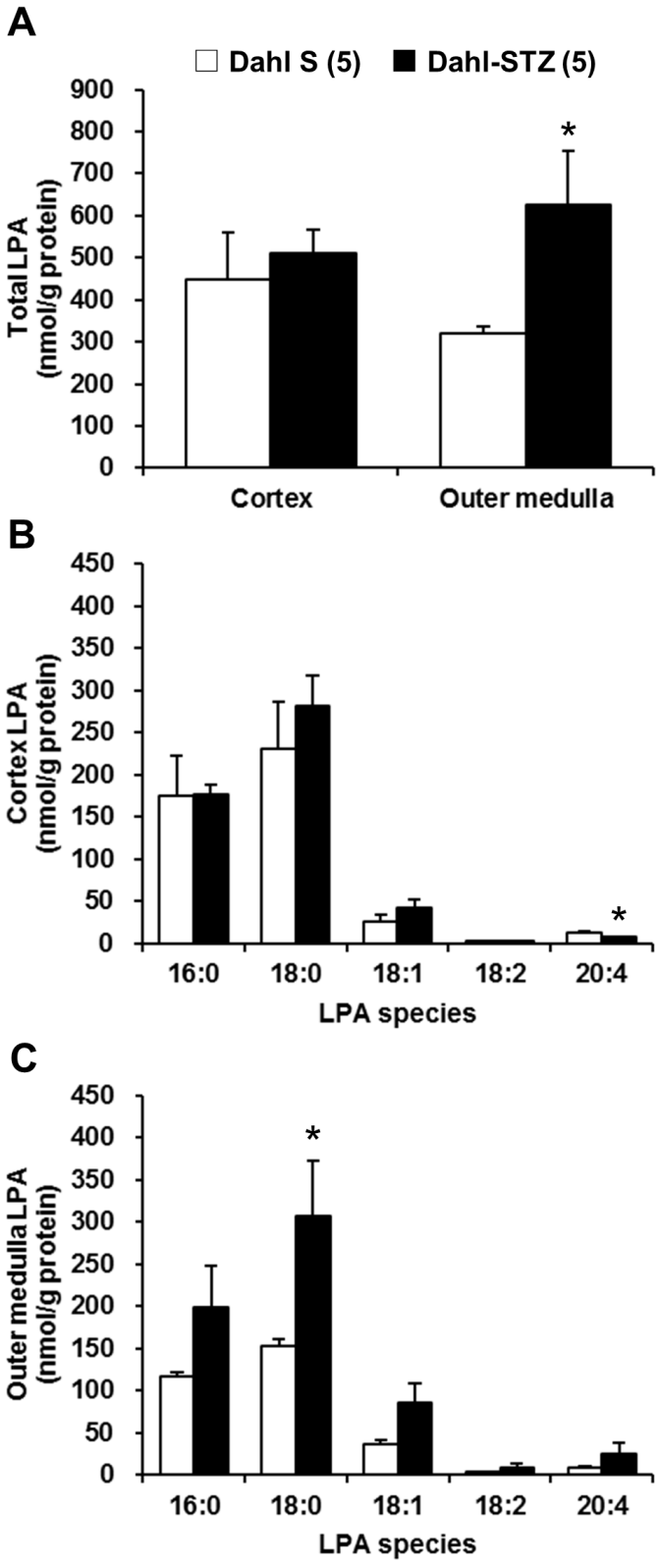

JPET Fast Forward. Published on December 4, 2020 as DOI: 10.1124/jpet.120.000353
This article has not been copyedited and formatted. The final version may differ from this version.

Figure 4

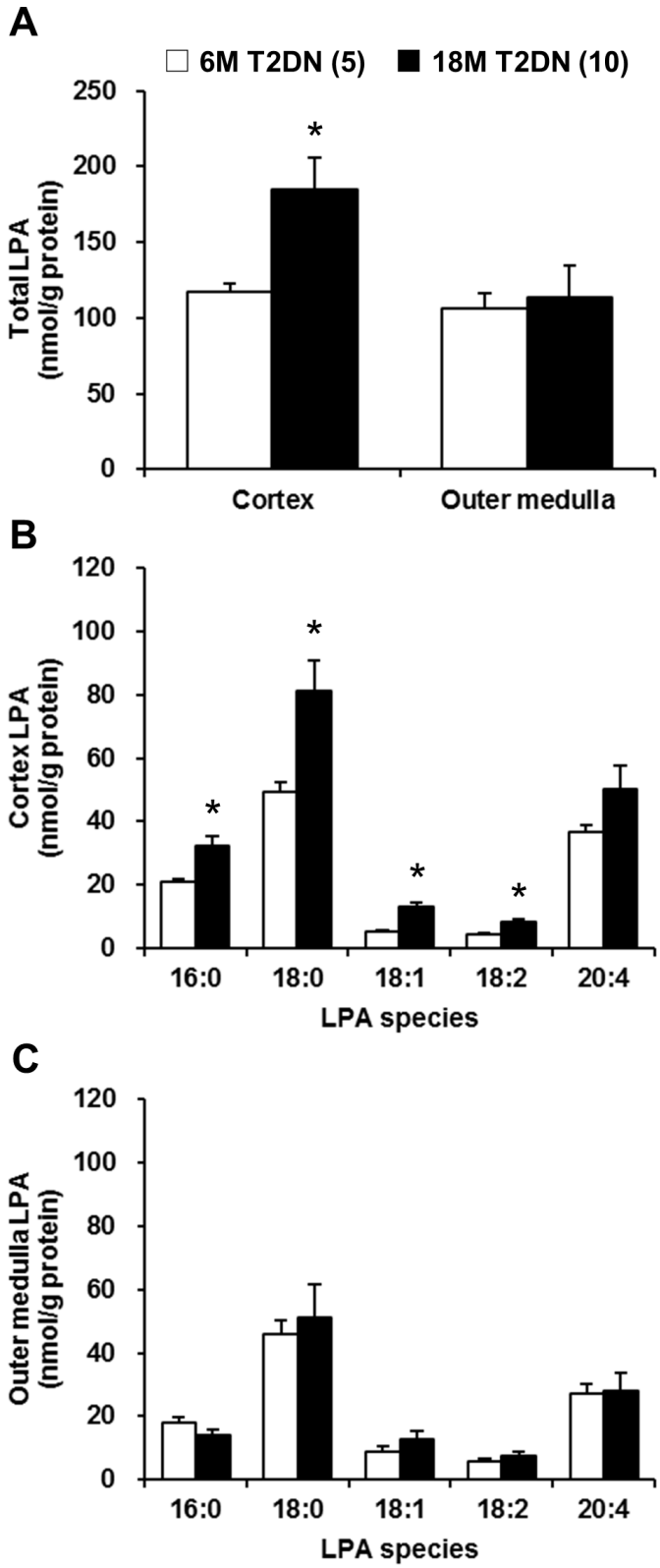

JPET Fast Forward. Published on December 4, 2020 as DOI: 10.1124/jpet.120.000353
This article has not been copyedited and formatted. The final version may differ from this version.

Figure 5

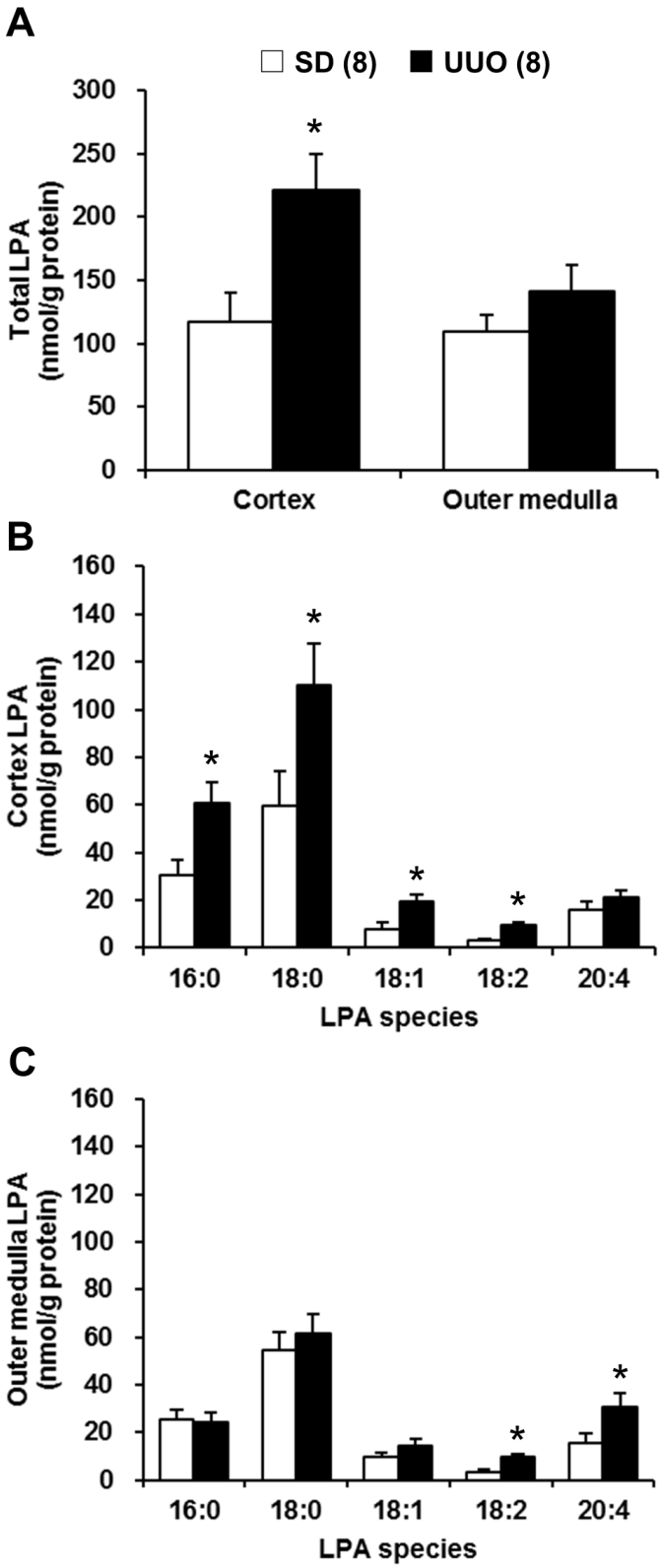

JPET Fast Forward. Published on December 4, 2020 as DOI: 10.1124/jpet.120.000353
This article has not been copyedited and formatted. The final version may differ from this version.

Figure 6

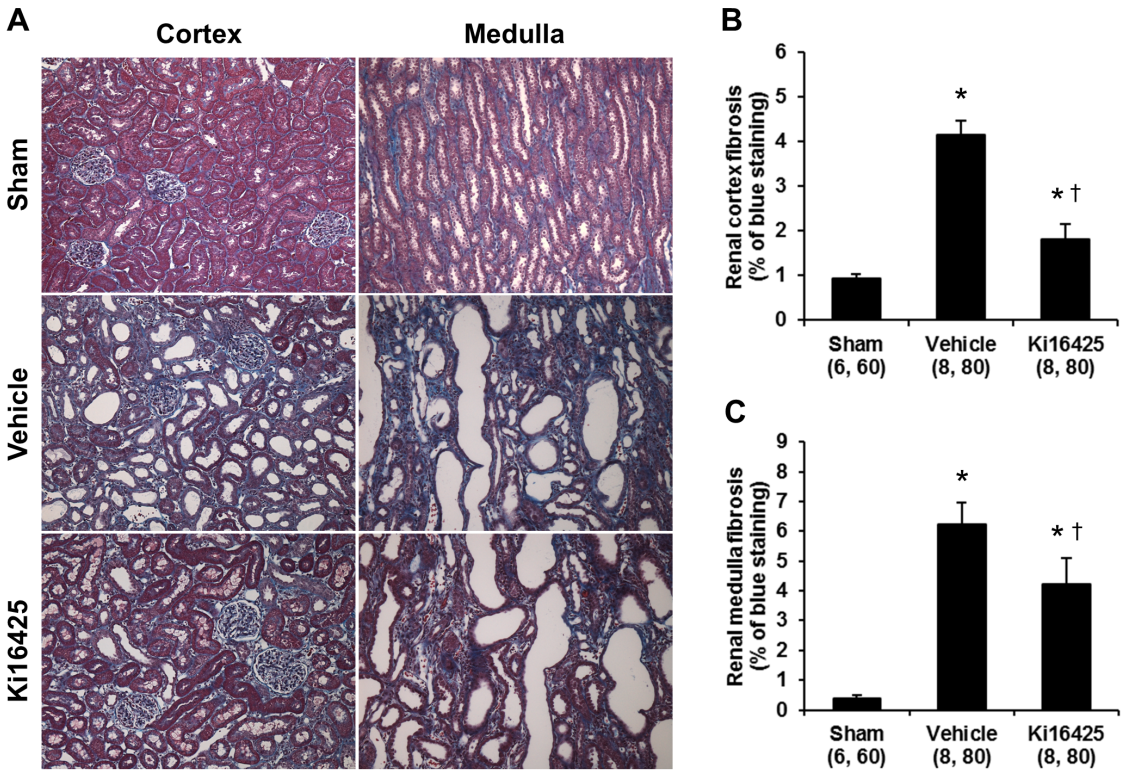

JPET Fast Forward. Published on December 4, 2020 as DOI: 10.1124/jpet.120.000353
This article has not been copyedited and formatted. The final version may differ from this version.

Figure 7